Analysis of enhanced modal damping ratio in porous materials using an acoustic-structure interaction model

Kook, Junghwan; Jensen, Jakob Søndergaard

Published in:
A I P Advances

Link to article, DOI:
10.1063/1.4901881

Publication date:
2014

Document Version
Publisher's PDF, also known as Version of record

AIP Advances

Analysis of enhanced modal damping ratio in porous materials using an acoustic-structure interaction model

Junghwan Kook and Jakob S. Jensen

Citation: AIP Advances **4**, 124304 (2014); doi: 10.1063/1.4901881
View online: http://dx.doi.org/10.1063/1.4901881
View Table of Contents: http://scitation.aip.org/content/aip/journal/adva/4/12?ver=pdfcov
Published by the AIP Publishing

Analysis of enhanced modal damping ratio in porous materials using an acoustic-structure interaction model

Junghwan Kook[1,a] and Jakob S. Jensen[2]
[1]*Department of Mechanical Engineering, Technical University of Denmark, Kgs. Lyngby, 2800, Denmark*
[2]*Department of Electrical Engineering, Technical University of Denmark, Kgs. Lyngby, 2800, Denmark*

(Received 15 September 2014; accepted 30 October 2014; published 13 November 2014)

The aim of this paper is to investigate the enhancement of the damping ratio of a structure with embedded microbeam resonators in air-filled internal cavities. In this context, we discuss theoretical aspects in the framework of the effective modal damping ratio (MDR) and derive an approximate relation expressing how an increased damping due to the acoustic medium surrounding the microbeam affect the MDR of the macrobeam. We further analyze the effect of including dissipation of the acoustic medium by using finite element (FE) analysis with acoustic-structure interaction (ASI) using a simple phenomenological acoustic loss model. An eigenvalue analysis is carried out to demonstrate the improvement of the damping characteristic of the macrobeam with the resonating microbeam in the lossy air and the results are compared to a forced vibration analysis for a macrobeam with one or multiple embedded microbeams. Finally we demonstrate the effect of randomness in terms of position and size of microbeams and discuss the difference between the phenomenological acoustic loss model and a full thermoacoustic model. [http://dx.doi.org/10.1063/1.4901881]

I. INTRODUCTION

In a simple experiment (see Figure 1) it was observed that beams made from a porous material fabricated using a selective laser melting possess higher modal damping ratios than beams of similar size made from a more homogeneous material.[1] Differences up to a factor of two were noticed, and the combination of low weight, high stiffness and favorable damping characteristics make these materials attractive for industrial applications where the damping of vibrations in the audible frequency range is of interest. The measurements were also supported by a notable difference in "ringing" when performing a simple drop test on a table, indicating an increased damping of the vibration modes in this frequency range.

In this paper we investigate to which extent the increased modal damping ratio can be ascribed to acoustic-structure interaction effects in the internal porosities due to resonantly vibrating structural microbeams. The vibrating microbeams are thought to represent either thin side walls or other small features in the porous material. It should be emphasized that the aim of the present study is not to perform a quantitative comparison with experiments, rather the experimental observations have served as a motivation for the theoretical and numerical study in this paper.

The reduction of structural vibrations using small resonating attachments has a long history of scientific and practical interest. The construction is commonly known as the tuned-mass damper and has widespread use for vibration damping in civil and mechanical engineering structures. Den Hartog's equal peak method[2] provides design guidelines for tuning the parameters of a vibrating attachment in terms of mass, stiffness coefficient and viscous damping coefficient, and research has

[a]Corresponding author, junko@elektro.dtu.dk

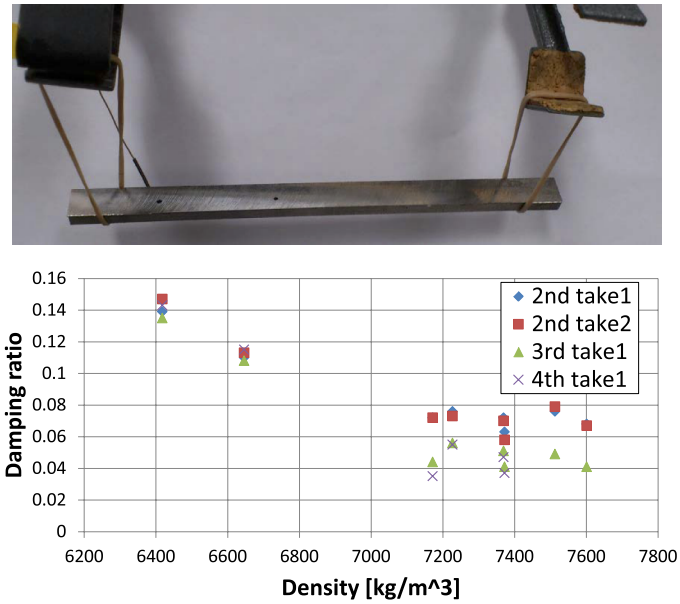

FIG. 1. Simple experimental setup for extracting the modal damping ratios for the 2.-4. vibration mode of a number of porous beams.[1] Beam dimensions; length: 175 mm, height: 5 mm, width: 10 mm. The beam was excited with a hammer and the response recorded with a small accelerometer. The experimental results serve as a motivation for the theoretical and numerical study in this paper.

continued in order to optimize the performance for different criteria and exact closed-form expressions for the optimal parameters have been developed.[3] Recently the equal peak method has been extended to cover also vibrations of nonlinear structures with arbitrary amplitude.[4] The use of multiple attachments – in the form of multiple tuned-mass dampers – has also been studied thoroughly using either a discrete[5] or a continuous description of the attachments.[6] The benefit of multiple dampers compared to a single damper being mainly the ability to control vibrations at a broader frequency range and not only in the near vicinity of a single frequency.

Recently, the properties of periodic configurations of internal resonators have been studied intensively – sometimes referred to as locally resonant material.[7] This material has demonstrated its use for control of low frequency vibrations and waves, and has been realized also in membrane-like structures for efficient shielding of low frequency noise.[8] With a periodic configuration of the resonators, bandgaps can appear in the bandstructure corresponding to forbidden frequency ranges for which waves cannot propagate though the materials.[9] Unlike, bandgaps effects based on wave interference, the forbidden frequencies appear at lower frequency ranges thus making them attractive for low frequency (audible) applications. It should be emphasized that the observed vibration reduction in finite samples is not restricted to a periodic assembly of resonators. Due to their attractive properties, significant research activities have been seen for locally resonant materials in the last 10 years, see e.g. Refs. 10 and 11 and they have also been studied by the second author of the present paper,[12] also in the case of nonlinear internal resonators.[13] Recently, the damping properties of structures with resonating elements were examined in detail.[14] For a comprehensive overview of the different bandgap phenomena see Ref. 15.

The model studied in this work is strongly inspired by the work on locally resonant material mentioned above. We will however, not rely on a strict periodic distribution of the resonating elements, but we will describe a porous material as a continuous ensemble of microbeams vibrating in acoustic cavities. Additionally, we will use an acoustic-structure interaction model in the numerical analysis to account for the damping of the vibrating microbeams. As we will show with a simple theoretical model, an increase in the overall modal damping ratio will rely on an increased damping of the microbeams due to the interaction effects. Such an increase has also been previously been reported in a study that showed an increased damping ratio of microbeams vibrating in small air cavities.[16]

The paper is organized as follows. In section II, we present a simple theoretical model that can provide an estimate of the effective modal damping ratio enhancement due to internal resonating microbeams. In section III we conduct a numerical acoustic-structure interaction study of a single microbeam in an air cavity and compute the modal damping ratios obtained with a phenomenological model for the acoustic losses. This study is then extended to compute the modal damping ratios for a macrobeam with one or multiple embedded microbeams. We study the forced vibrations of a macrobeam with a single and a finite number of microbeams, also for the case of a random location and thickness of the microbeams. Finally, we compare the results using the phenomenological model to an acoustic-structure interaction study using a full thermoacoustic model. In section IV we present the conclusions.

II. THEORETICAL MODEL

In this section we will derive a simple formula for predicting the effective increase in the macroscopic modal damping ratio due to a number of resonating microbeams embedded in the macrobeam. The model will be based on a known microscopic damping ratio of the vibrating microbeams. The main assumption in the following is that the microbeams are homogenously spread in the macrobeam and are sufficiently small so that the macrobeam mode shapes are not significantly altered by their motion.

The motion of the macrobeam is then, with a good approximation, characterized by the standard set of mode shapes $\varphi_j(x)$ and natural frequencies Ω_j. We will study resonant vibrations of the macrobeam, so we will consider only a single mode in the expansion. The macrobeam motion can therefore be written as

$$\omega(x,t) = q_j \varphi_j(x) \cos \Omega_j t \tag{1}$$

where q_j is an unknown modal amplitude. In the following the subscript j will be omitted for brevity.

A. Microbeam model

We now look at the motion of a single microbeam embedded into the macrobeam. We assume that the beam is sufficiently slender so that the Bernoulli-Euler beam theory can be applied and the equation of motion for a microbeam of mass density ρ and Young's modulus E is then given as:

$$\rho A_m \ddot{\tilde{u}} + c_m \dot{u} + E I_m u'''' = 0 \tag{2}$$

where $\ddot{\tilde{u}}$ is the total transverse acceleration of the beam, A_m is its cross sectional area, I_m the moment of inertia and c_m a viscous damping coefficient. In (2) dots refer to time derivatives and primes to space derivatives. The microbeam is excited by the motion of the macrobeam, thus the total acceleration $\ddot{\tilde{u}}$ can be written as a sum of the acceleration relative to the motion of the macrobeam and the acceleration of the macrobeam at the location of the microbeam:

$$\ddot{\tilde{u}}(x_m,t) = \ddot{w}(x_p,t) + \ddot{u}(x_m,t) \tag{3}$$

where x_p denotes the location of the microbeam. Inserting (3) into (2) and with the single mode expansion in (1) yields:

$$\rho A_m \ddot{u} + c_m \dot{u} + E I_m u'''' = \rho A_m \Omega^2 q \varphi_p e^{i\Omega t} \tag{4}$$

which represents the forced vibration problem of a single microbeam.

We will restrict ourselves to consider low mode macrobeam motion with an angular frequency Ω that is in the vicinity of the fundamental natural frequency of the microbeam. Thus we can approximate the microbeam motion using a single mode expansion (using a complex notation):

$$u(x_m,t) = y \phi(x_m) e^{i\Omega t} \tag{5}$$

where y is the unknown (complex) modal amplitude and $\phi(x_m)$ is the fundamental mode shape of the microbeam found by solving the linear eigenvalue problem corresponding to (4) with $\ddot{u} = q = 0$.

Inserting the expansion in (5) into (4) yields:

$$-\rho A_m \Omega^2 y\phi e^{i\Omega t} + i\Omega c_m y\phi e^{i\Omega t} + EI_m y\phi'''' e^{i\Omega t} = \rho A_m \Omega^2 q\varphi_p e^{i\Omega t} \tag{6}$$

where the explicit dependence of the mode shape ϕ on the coordinate x_m has been omitted and the short notation $\varphi_p = \varphi(x_p)$ has been applied as well.

Now we apply a standard Galerkin procedure by premultiplying the expression in (6) by ϕ, integrating over the length of the microbeam (L_m), and utilizing the properties of the microbeam modehapes: $\int_0^{L_m} \phi^2 dx_m = L_m$ (for a clamped-clamped or cantilever beam), as well as $\int_0^{L_m} \phi\phi'''' dx_m = L_m\omega^2\rho A_m/EI_m$ where ω is the fundamental eigenfrequency

$$-L_m\rho A_m\Omega^2 y + L_m i\Omega c_m y + L_m\omega^2\rho A_m y = L_m\sigma\rho A_m\Omega^2 q\varphi_p \tag{7}$$

where the factor $\int_0^{L_m} \phi dx_m = \sigma L_m$, σ depending on the boundary conditions of the microbeam, has been introduced as well. The expression in (7) can further be simplified as:

$$-(\frac{\Omega}{\omega})^2 y + i\frac{\Omega}{\omega}\frac{c_m}{\rho A_m\omega} y + y = \sigma(\frac{\Omega}{\omega})^2 q\varphi_p \tag{8}$$

and by introducing the non-dimensional frequency $\tilde{\Omega} = \Omega/\omega$ and the non-dimensional damping parameter $\zeta_m = c_m/2\rho A_m\omega$ written as:

$$-\tilde{\Omega}^2 y + 2i\tilde{\Omega}\zeta_m y + y = \sigma\tilde{\Omega}^2 q\varphi(x_p) \tag{9}$$

which we can now solve for the complex modal amplitude y.

$$y = \frac{\sigma\tilde{\Omega}^2\varphi(x_p)}{(1-\tilde{\Omega}^2) + 2i\tilde{\Omega}\zeta_m} q \tag{10}$$

The ratio between the squared modal amplitude of a microbeam and the squared modal amplitude of the macrobeam will be needed in the following and is given as

$$\frac{|y|^2}{q^2} = \frac{\sigma^2\tilde{\Omega}^4\varphi_p^2}{(1-\tilde{\Omega}^2)^2 + 4\zeta_m^2\tilde{\Omega}^2} \tag{11}$$

B. Effective modal damping ratio

We will now use the expression for the microbeam modal amplitude to develop an expression for the effective modal damping ratio of the macrobeam. The effective modal damping ratio will be expressed in terms of a magnification factor ζ_{eff}/ζ, which will take a unity value if the macrobeam does not have internal vibrating microbeams. As will be shown in the following, the magnification factor will also take the value unity if the damping ratio of the microbeam ζ_m equals the damping ratio of the macrobeam ζ, thus we predict that effective modal damping ratio is only increased if the internal damping ratio is higher than the ambient damping ratio. However, as also mentioned in the introduction, this is indeed to be expected due to the acoustic-structure interaction enhanced by the small size of the cavities.

The effective damping ratio is computed as follows

$$\zeta_{eff} = \frac{1}{4\pi}\frac{\Delta W}{W} \tag{12}$$

in which W is the maximum stored potential energy in the system and ΔW is the energy dissipated in the system during an excitation cycle:

The maximum stored potential energy we can write as the sum of the contribution from the macrobeam and the microbeams:

$$W = \tfrac{1}{2}\int_0^L w_{max}\tilde{E}Iw''''_{max}dx + \sum_{p=1}^{N}\tfrac{1}{2}\int_0^{L_m} u_{max}EI_m u''''_{max}dx_m \tag{13}$$

where $\tilde{E}I$ is the effective bending stiffness of the macrobeam and where we assume that also the macrobeam is sufficiently slender so that the Bernoulli-Euler theory can be applied. Expanding the equation we obtain

$$W = \tfrac{1}{2}\tilde{E}Iq^2\int_0^L \varphi\varphi''''dx + \sum_{p=1}^{N}\tfrac{1}{2}EI_m|y_p|^2\int_0^l \phi\phi''''dx_m = \tfrac{1}{2}q^2L\Omega^2\tilde{\rho}A + \sum_{p=1}^{N}\tfrac{1}{2}|y|^2L_m\omega^2\rho A_m \tag{14}$$

The total dissipated energy is also the sum of the dissipation in the macro- and microbeams. The contribution from the microbeams can be computed as

$$\Delta W_{mic} = \sum_{p=1}^{N}\int_0^{L_m}\int_0^{\frac{2\pi}{\Omega}} \Re(\dot{u})c_m\Re(\dot{u})dtdx \tag{15}$$

where $\Re()$ denotes the real part of the term. By inserting the expressions and simplifying we obtain

$$\Delta W_{mic} = \sum_{p=1}^{N} c_m\Omega^2\frac{\pi}{\Omega}|y|^2\int_0^{L_m}\phi^2dx = \pi\Omega\sum_{p=1}^{N}c_m|y|^2L_m \tag{16}$$

In a similar way we can compute the dissipated energy in the macrobeam as:

$$\Delta W_{mac} = \int_0^L\int_0^{\frac{2\pi}{\Omega}} \Re(\dot{w})c\Re(\dot{w})dtdx \tag{17}$$

where c is a viscous damping coefficient for the motion of the macrobeam. The dissipated energy can be expressed in terms of the modal amplitude by inserting the expression in (1):

$$\Delta W_{mac} = c\Omega^2\int_0^L\int_0^{\frac{2\pi}{\Omega}}\varphi^2q^2\sin^2\Omega t dtdx = \pi\Omega cq^2L \tag{18}$$

We can now collect all contributions and obtain an expression for the effective loss factor:

$$\zeta_{eff} = \frac{1}{4\pi}\frac{\pi\Omega(cLq^2 + \sum c_mL_m|y|^2)}{\frac{1}{2}q^2L\Omega^2\tilde{\rho}A + \sum\frac{1}{2}|y|^2L_m\omega^2\rho A_m} \tag{19}$$

To proceed we will now make the crude assumption that all microbeams have identical properties. This allows us to divide the expressions by ω^2, L_m and ρA_m and results in the following expresssion:

$$\zeta_{eff} = \tfrac{1}{2}\frac{\frac{\Omega}{\omega}(\frac{c}{\Omega\tilde{\rho}A}\frac{\tilde{\rho}A}{\rho A_m}\frac{\Omega}{\omega}\frac{L}{L_m}q^2 + \sum\frac{c_m}{\omega\rho A_m}|y|^2)}{q^2\frac{L}{L_m}\frac{\Omega^2}{\omega^2}\frac{\tilde{\rho}A}{\rho A_m} + \sum|y|^2} \tag{20}$$

We can then introduce the internal and external modal damping ratios, where the latter is defined as $\zeta = c/(2\tilde{\rho}A\Omega)$ with $\tilde{\rho}A$ being the effective mass per length:

$$\zeta_{eff} = \tfrac{1}{2}\frac{\tilde{\Omega}(2\zeta\frac{\tilde{\rho}A}{\rho A_m}\tilde{\Omega}\frac{L}{L_m}q^2 + \sum 2\zeta_m|y|^2)}{q^2\frac{L}{L_m}\tilde{\Omega}^2\frac{\tilde{\rho}A}{\rho A_m} + \sum|y|^2} \tag{21}$$

It is now convenient to introduce the non-dimensional mass ratio

$$\tilde{m} = \frac{\tilde{\rho}AL}{\rho A_mL_m} \tag{22}$$

that represents the ratio between the total beam mass and that of a single micro resonator. Inserting also the expression for the squared modal amplitude yields

$$\frac{\zeta_{eff}}{\zeta} = \frac{\tilde{m}\tilde{\Omega}^2 + \sum \frac{\zeta_m}{\zeta}\tilde{\Omega}\frac{\sigma^2\tilde{\Omega}^4\varphi_p^2}{(1-\tilde{\Omega}^2)^2 + 4\zeta_m^2\tilde{\Omega}^2}}{\tilde{m}\tilde{\Omega}^2 + \sum \frac{\sigma^2\tilde{\Omega}^4\varphi_p^2}{(1-\tilde{\Omega}^2)^2 + 4\zeta_m^2\tilde{\Omega}^2}} \tag{23}$$

It is clear from (23) that an enhancement of the global modal damping ratio relies on the damping ratio for the microbeams being higher than the external damping ratio ($\zeta_m/\zeta > 1$). In the case when $\zeta_m/\zeta = 1$ (and resonant conditions: $\tilde{\Omega} \approx 1$) then $\zeta_{eff}/\zeta \approx 1$ and no enhancement is obtained.

We will now make a few assumptions to simplify the equation. Firstly, we assume that the number of microresonators N is large and that they are evenly distributed along the macrobeam. In this way

$$\sum_{p=1}^{N} \varphi_p^2 \approx \frac{N}{L_m}\int_0^{L_m} \varphi^2(x_p)dx_m = N \tag{24}$$

Additionally, we will introduce the non-dimensional mass parameter α that quantifies the ratio between the macrobeam mass and the total mass of resonating microbeam

$$\alpha = \frac{\tilde{\rho}AL}{N \times \rho A_m L_m} = \frac{\tilde{m}}{N} \tag{25}$$

then the expression simplifies to

$$\frac{\zeta_{eff}}{\zeta} = \frac{\alpha\tilde{\Omega}^2 + \frac{\zeta_m}{\zeta}\tilde{\Omega}\frac{\sigma^2\tilde{\Omega}^4}{(1-\tilde{\Omega}^2)^2 + 4\zeta_m^2\tilde{\Omega}^2}}{\alpha\tilde{\Omega}^2 + \frac{\sigma^2\tilde{\Omega}^4}{(1-\tilde{\Omega}^2)^2 + 4\zeta_m^2\tilde{\Omega}^2}} \tag{26}$$

The enhancement effect is largest in the vicinity of perfect tuning of the microbeams to the resonant motion, i.e. when $\tilde{\Omega} \approx 1$. For this special case, we obtain the simple formula

$$\frac{\zeta_{eff}}{\zeta} = \frac{\alpha + \frac{\zeta_m}{\zeta}\frac{\sigma^2}{4\zeta_m^2}}{\alpha + \frac{\sigma^2}{4\zeta_m^2}} \tag{27}$$

in which it is more convenient to introduce ζ as the free parameter and we thus arrive at the final expression:

$$\frac{\zeta_{eff}}{\zeta} = \frac{\alpha + \frac{\sigma^2}{4\zeta^2\tilde{\zeta}_m}}{\alpha + \frac{\sigma^2}{4\zeta^2\tilde{\zeta}_m^2}} \tag{28}$$

where $\tilde{\zeta}_m = \zeta_m/\zeta$. As indicated in the derivation above, this very simple formula is derived with assumption that all microbeams are equal and vibrating at resonance. This is of course far from realistic for a porous material. However, the effect of the associated error can to some extent be compensated for by a proper choice of the parameter α, which should then be interpreted at the total mass the beam relative to the mass of those microbeams that vibrate at resonance.

C. Numerical example

We now consider a numerical example where we consider the microbeams as clamped-clamped (corresponding to $\sigma = 0.83$) and we plot the magnification factor ζ_{eff}/ζ as a function of the ratio of internal to external damping $\tilde{\zeta}_m$ in Figure 2. For three different values of the external damping ratio ζ we show the magnification factor for three values of the mass parameter α.

It is clear that for a small value of ζ then the relative enhancement is larger than for a more strongly externally damped structures. Also the effect of the mass ratio α is less pronounced when the structure is lightly damped. In the case of a real porous beam, the parameter α is expected

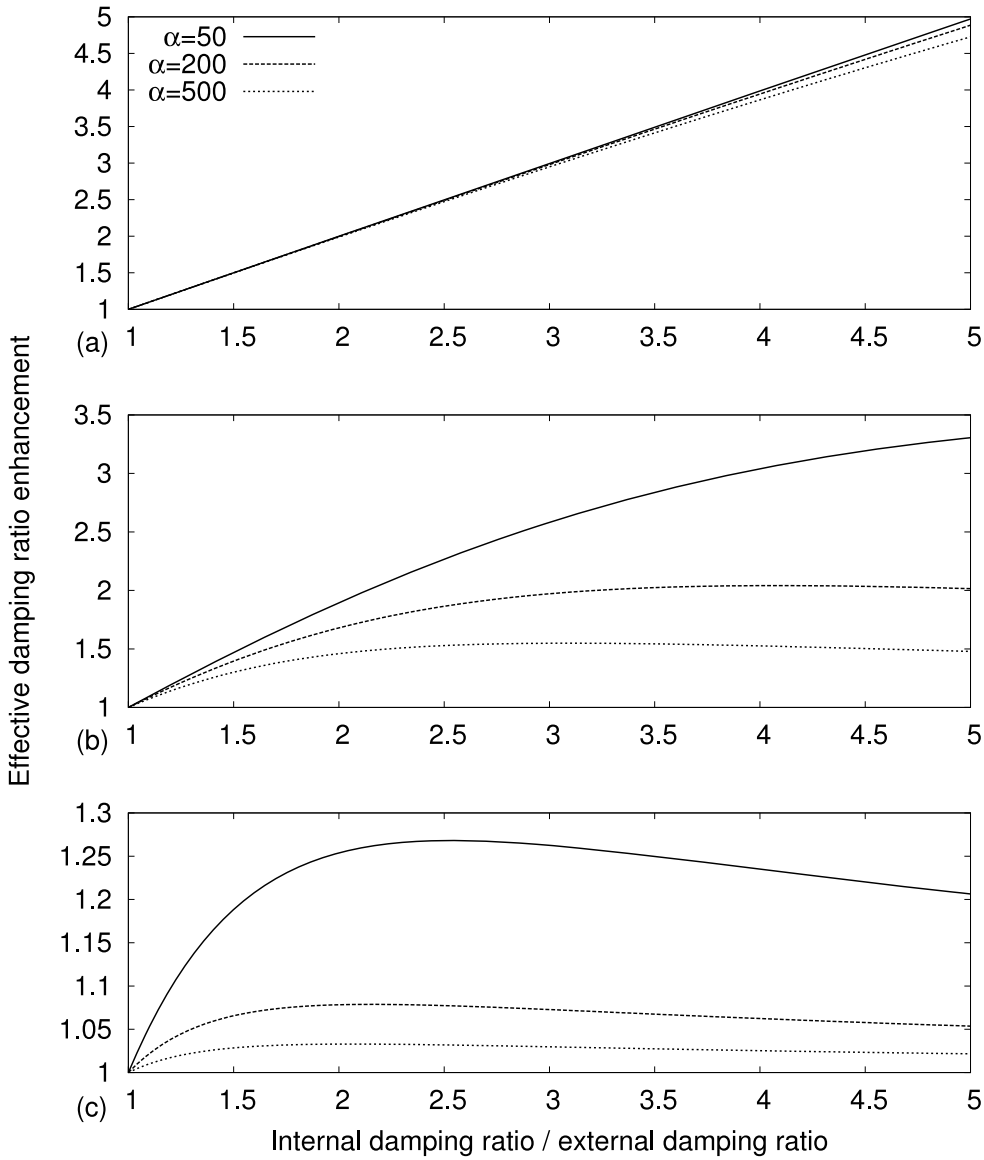

FIG. 2. The enhancement of the effective modal damping ratio as a function of the ratio between the internal and external viscous damping ratio for different values of the external viscous damping ratio, (top) ζ=0.001, (middle) ζ=0.01, (bottom) ζ=0.05.

to large. However, we can see from Figure 2 (top), that for low external damping (0.1%), we predict that an increased internal damping is directly reflected in an increase in the magnification factor – thus the experimental observation of a factor two in enhancement would not be unrealistic.

III. NUMERICAL ACOUSTIC-STRUCTURE INTERACTION STUDY

In the following we will further study the enhancement effect using a FE model with acoustic-structure interaction in the air cavities. For computational reasons we will have only small number of embedded microbeams (starting with one!) and thus the results will not be directly comparable with the theoretical model.

First, a numerical experiment for a 2-dimensional macrobeam with one single microbeam resonator is presented (Figure 3). We tune the geometrical and material properties to match the 1st bending mode of the microbeam to the 1st bending mode of the macrobeam. This is accomplished

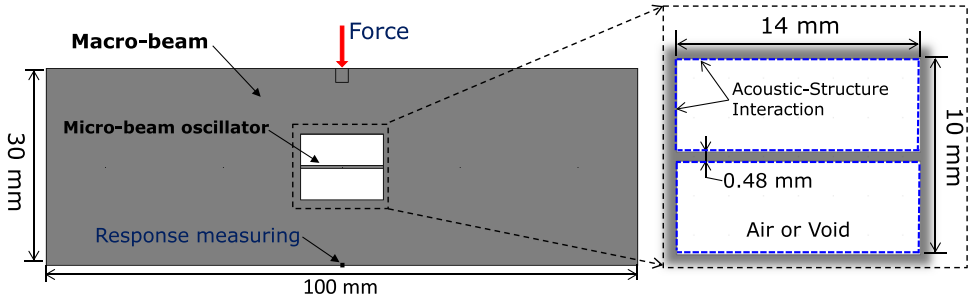

FIG. 3. Geometry for a macrobeam structure with a microbeam resonator in a cavity. The cavity is filled with air or empty (void).

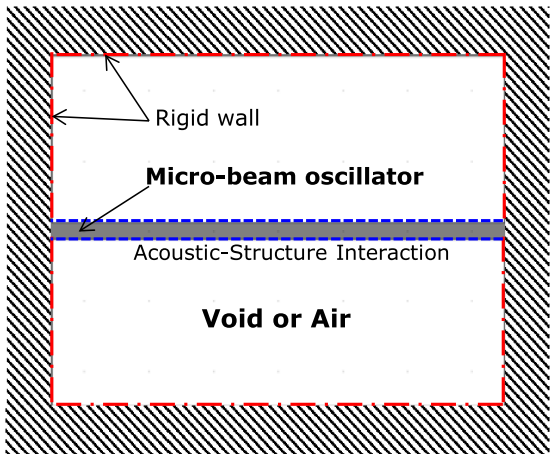

FIG. 4. The model for the microbeam resonator placed in a cavity. The rigid wall condition is imposed on the boundary with the red dashed line.

by a macrobeam of 30 mm and 100 mm height and length, respectively, an acoustic cavity of 14 mm x 10 mm and a microbeam with thickness = 0.48 mm (located in the middle of the cavity). A Young's modulus E_0 of 2 GPa, and the mass density, ρ is 1000 Kg/m^3 has been arbitrarily chosen. For overall damping we use a complex Young's modulus, so that $E_c = E_0(1 + i\eta_{sol})$. In all examples in this paper we employ the structural damping as $\eta_{sol} = 1.0e - 03$.

As a first approach to model a lossy acoustic medium we apply a complex speed of sound on the form $c_c = c_0(1 + i\eta_{air})$, where η_{air} is an acoustic loss factor. We employ values of η_{air} as 0.0, 0.01, and 0.1, respectively. The speed of sound c_0 is 343 m/s, and the air density ρ_{air} is 1.25 Kg/m^3. We employ finite element analysis with an acoustic-structure interaction (ASI) model and all analyses are carried out using the commercial software package COMSOL Multi-physics.[17]

It should be noted that, in general, dissipation or damping in an acoustic medium takes place through interaction with solids, either because of friction between the fluid and a porous material filling the domain, or because acoustic energy is transferred to a surrounding solid where it is absorbed. In addition, in systems with small length scales, significant losses can occur in the viscous and thermal acoustic boundary layer at walls. However, the phenomenological model provides a straightforward approach to investigate the enhancement of the damping property of a structure with embedded microbeam resonators in air-filled internal cavities. The model is computationally much less heavy than solving full poroelastic or thermoacoustics model. In order to include the losses in the acoustic medium in a more detailed way, a numerical example using the thermoacoustic-structure interaction model is examined in Section III D and the result will be discussed and compared with phenomenological model.

TABLE I. Results of the eigenvalue analyses for the microbeam resonator placed in the air-filled cavity including different dissipation in the air.

Eigen Solution	Beam only (No Air)	Acoustic Structure Interaction		
		$\eta_{air} = 0.0$	$\eta_{air} = 0.01$	$\eta_{air} = 0.1$
ω_1	2.3554e+04	2.5335e+04	2.5335e+04	2.5320e+04
α_1	1.1777e+01	1.0933e+01	4.5626e+01	3.5808e+02
ζ_1	5.0000e-04	4.3153e-04	1.8009e-03	1.4140e-02
ω_2	6.4198e+04	6.3060e+04	6.3061e+04	6.3227e+04
α_2	3.2099e+01	2.9427e+01	7.1415e+01	3.7309e+02
ζ_2	5.0000e-04	4.6665e-04	1.1325e-03	5.9007e-03

First, an eigenvalue analysis is carried out. The eigenvalue problem yields a set of complex values $\lambda_i = \pm\sqrt{\beta_i} = \omega_i + i\alpha_i$, where $\mathrm{Re}(\lambda_i) = \omega_i$ and $\mathrm{Im}(\lambda_i) = \alpha_i$. Thus, the MDR corresponding to the i^{th} eigenfrequency is obtained by

$$\varsigma = \frac{\alpha_i}{\sqrt{\alpha_i^2 + \omega_i^2}} \tag{29}$$

For comparative purpose, we compute the MDR without the dissipation in the acoustic media as well as for a macrobeam with voids instead of acoustic cavities.

A. Microbeam submerged in an air-filled internal cavity

First we investigate the isolated behavior of a microbeam vibrating in an air-filled cavity. The dimensions of the microbeam and the air cavity are the same as seen in Figure 3 and also the material properties are unchanged. However, the boundary conditions on the walls of the acoustic cavity are changed to being rigid (or hard) wall seen in Figure 4.

Table I summarizes the results of the analysis. The computed MDR for the void case are $\eta_{sol}/2$ = 5.000e-04 for the first and second modes. In case of the ASI simulations, it shows that the MDR is significantly enhanced compared to the void case at the both modes. For the fundamental mode, i.e. the 1st bending mode, the improvements are 260% and 2728% with respect to the void model, respectively. The results clearly shows that the inclusion of air dissipation has a direct impact on the MDR of the microbeam. Additionally, we see that the real part of the 1st eigenfrequency is slightly increased while the real part of the 2nd eigenfrequency is decreased. The changes in resonant frequencies in the ASI model result from various factors, such as equivalent mass/stiffness/damping resulting of acoustic coupling for each mode shape of the microbeam, seen in Figure 5. We note that when the anti-modal line or modal line of acoustic pressure is parallel to a vibrating microbeam, the presence of the air exerts a strong influence on the MDR of the microbeam. This effect is further enhanced when acoustic modes lie in the vicinity of the structural modes, which is not the case here (the eigenfrequency of the 1st acoustic mode is around

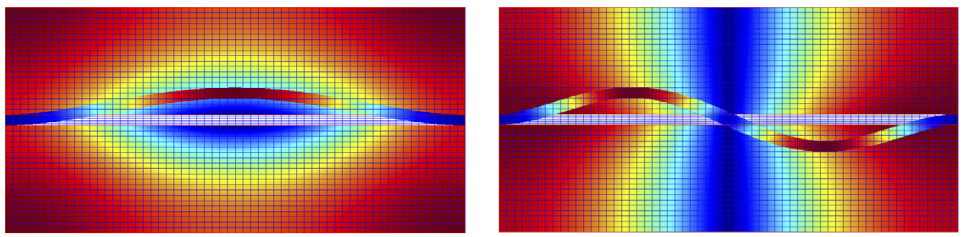

FIG. 5. Mode shape of the microbeam and the acoustic pressure contour interacting with the microbeam mode: (left) the 1st mode shape (right) the 2nd mode shape.

TABLE II. Results of the eigenvalue analyses for the macrobeam with a microbeam resonator in an air-filled internal cavity including dissipation in the air. The superscript indicates the order of the microbeam mode.

Eigen Solution	Void (No Air)	Acoustic Structure Interaction		
		η_{air} = 0.0	η_{air} = 0.01	η_{air} = 0.1
ω_1	[1,]2.2174e+04	2.3154e+04	2.3154e+04	2.3167e+04
α_1	[1,]1.1086e+01	1.1187e+01	1.8973e+01	8.7968e+01
ς_1	[1,]5.0000e-04	4.8319e-04	8.1943e-04	3.8032e-03
ω_2	2.3715e+04	[1,]2.4580e+04	[1,]2.4580e+04	[1,]2.4552e+04
α_2	1.1857e+01	[1,]1.0818e+01	[1,]4.0592e+01	[1,]3.0656e+02
ς_2	5.0000e-04	[1,]4.4011e-04	[1,]1.6379e-03	[1,]1.2485e-02
ω_3	3.4697e+04	3.4526e+04	3.4526e+04	3.4526e+04
α_3	1.7348e+01	1.7263e+01	1.7264e+01	1.7277e+01
ς_3	5.0000e-04	5.0000e-04	5.0004e-04	5.0041e-04
ω_4	4.1086e+04	4.1792e+04	4.1792e+04	4.1792e+04
ω_4	2.0903e+01	2.0896e+01	2.0898e+01	2.0926e+01
ς_4	5.0000e-04	5.0000e-04	5.0007e-4	5.0072e-04
ω_5	[2,]6.1086e+04	[2,]5.9934e+04	[2,]5.9935e+04	[2,]6.0031e+04
α_5	[2,]3.0543e+01	[2,]2.8603e+01	[2,]5.5838e+01	[2,]2.6279e+02
ς_5	[2,]5.0000e-04	[2,]4.7725e-04	[2,]9.3165e-04	[2,]4.3775e-03
ω_6	7.5100e+04	7.5043e+04	7.5043e+04	7.5043e+04
α_6	3.7550e+01	3.7518e+01	3.7599e+04	3.8333
ς_6	5.0000e-04	4.9994e-04	5.0103e-04	5.1081e-04

7.7e+04~7.8e+04 [rad/s], which is far away from the microbeam modes of interest). A further study of this will be left for future work.

B. Macrobeam with a microbeam resonator in an air-filled internal cavity

Having examined the damping property of the microbeam resonator itself, we will return to the issue of the enhancement of the MDR of the structure with the embedded microbeam. The results of the eigenvalue analyses shown in Table II demonstrate the enhancement of the damping characteristic of the macrobeam (spurious and rigid body modes have been excluded). The first 6 modes of each study case are obtained for the comparison and these are separated into 4 global modes (macrobeam modes) and the first 2 modes involving primarily microbeam motion (microbeam modes). The results are summarized in Table II.

We have tuned the model so that the 1st bending mode for the microbeam is close to the 1st bending mode of the macrobeam. Although the frequencies are not perfectly matched, this will be sufficient to demonstrate the enhancement of the damping.

In order to investigate the enhancement of the MDR for the 1st bending mode of the macrobeam, its corresponding eigenfrequency should be identified. Here we note that the order of the 1st bending mode of the macrobeam and the 1st bending mode of the microbeam is interchanged in comparison with the mode shapes of the void model. We focus our attention on the 1st bending mode of the macrobeam where we expect to observe enhancement in the damping compared to the void model. In the ASI model, it is observed that the MDRs with dissipation in the air have been increased from 5e-04 to 8.1943e-04 (η_{air} = 0.01) and 3.8032e-03 (η_{air} = 0.1), respectively. This corresponds to about 64% and 606% improvement, respectively. Additionally, it is noted from Table II that none of the other macrobeam modes display any significant increase in MDR, since they do not reside near any microbeam resonances. The 5th eigenfrequency corresponds to the second bending mode of the microbeam and the MDRs for the ASI model with dissipation are increased as was also seen with the previous results for the microbeam shown in Table I.

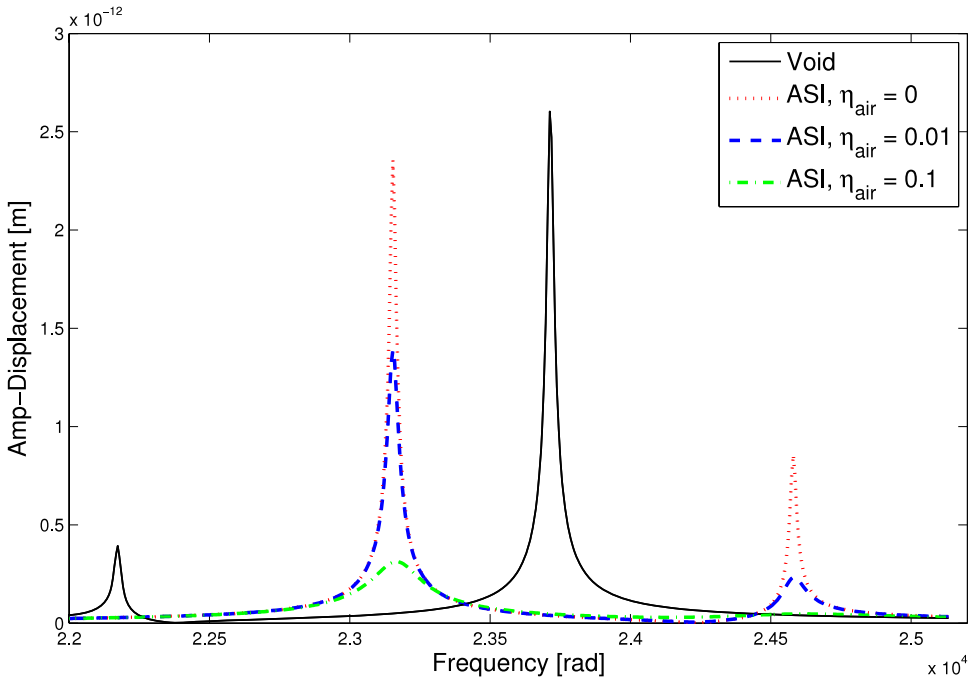

FIG. 6. Frequency responses for the macrobeam with a single microbeam resonator.

In order to see the effect of the enhanced MDR, we additionally perform a time-harmonic analysis of the macrobeam and study the frequency responses. As seen in Figure 3, a load 1 N is employed and the magnitude of y-displacement is examined at the response measuring point. The frequency spans a range from 2.2e+04 to 2.51e+04 [rad/s] computed at 2π [rad] intervals, which covers the first 2 eigenfrequencies. The results appear in Figure 6. It is seen that the location of all peaks in the frequency of interest correspond to the eigenfrequencies discussed in Table II, also indicating that the order of the first macro- and microbeam modes are interchanged when the dissipation is added. In the void model, we can see two sharp peaks at the two eigenfrequencies. When including the dissipation in air, we obtain the smoothed peak at the eigenfrequency due to the enhanced MDRs supporting the results from the eigenvalue analysis. If we compute the MDR based on the half power response we also get a close agreement.

C. Macrobeam with multiple microbeams

In the next example, we present the numerical results for a macrobeam with evenly distributed microbeam resonators. Figure 9 shows the geometry of the macrobeam and a total of 17 microbeam resonators evenly distributed. In this example, we set the geometry to make the 1st bending mode of the microbeam close to the 2nd bending mode of the macrobeam. The size of the macrobeam is 100 mm x 320 mm, the acoustic cavity is 20 mm x 20 mm and a microbeam with thickness = 0.4 mm. The positioning of the microbeams is seen in Figure 7. The material properties are unchanged.

First we compute the properties of the microbeam vibrating in an air-filled cavity. Table III shows the results with respect to the fundamental mode of the microbeam and the conclusion is similar to the one made in Section III.A for the microbeam with different geometry. The real part of the first eigenfrequency of the ASI models is about 1.1948e+04 and that of the void model is 9.7017e+03. When comparing the results in Table I, it shows a larger frequency shift upwards due to the microbeam being longer and thinner than the microbeam discussed in Section III.A and III.B. Consequently, we have set up the ASI model with the eigenfrequency of the 1st bending mode of the microbeam close to the 2nd bending mode for the macrobeam.

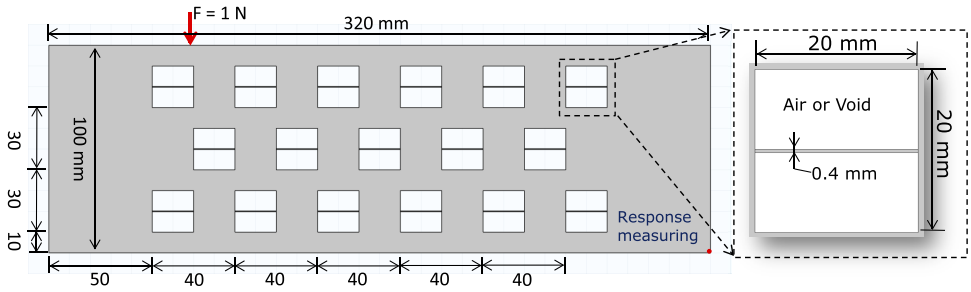

FIG. 7. Geometry for a macrobeam structure with 17 microbeam resonators with a cavity. Each cavity is filled with air or nothing (void).

TABLE III. The fundamental eigenfrequency and the its MDR for the microbeam resonator.

Eigen Solution	Beam only (No Air)	Acoustic Structure Interaction		
		$\eta_{air} = 0.0$	$\eta_{air} = 0.01$	$\eta_{air} = 0.1$
ω_1	9.7017e+03	1.1948e+04	1.1948e+04	1.1935e+04
α_1	4.8501e+00	3.8679e+00	4.5992e+01	4.2561e+02
ς_1	5.0000e-04	3.2372e-04	3.8493e-03	3.5638e-02

Now, the eigenvalue analysis of the macrobeam is carried out to investigate enhancement of the MDRs and the result for the void model is summarized in Table IV. In the case of the void model, 21 eigenfrequencies including 17 eigenfrequency for the microbeam mode are obtained. Table V shows the results for the ASI models with dissipation in the air. Due to the many microbeams the results of the eigenfrequency analysis is more complex and difficult to interpret. Again, the order of the eigenfrequencies has been changed in comparison with the void model. There are two eigenfrequencies that involve the 2nd bending mode of the macrobeam combined with the 1st bending mode of the microbeam (the 3rd eigenfrequency that is dominated by macrobeam motion and the 21nd eigenfrequency dominated by microbeam motion). In the close frequency neighborhood are 16 pure microbeam modes ranked 4th ~ 20th eigenfrequency. For the 3rd eigenfrequency, which can be described as the main macrobeam 2nd bending mode, the computed MDRs have been significantly

TABLE IV. The eigenfrequencies and MDRs for the macrobeam with 17 microbeams and void cavity.

Eigen Solution	Void (No Air)	Mode shape
ω_1	5.8447e+03	1st Bending mode
α_1	2.9224e+00	
ς_1	5.0000e-04	
$\omega_{2\sim18}$	9.4857e+03~9.5493e+03	17 microbeam modes (1st bending)
$\alpha_{2\sim18}$	4.7508+00~4.7693e+00	
$\varsigma_{2\sim18}$	5.0000e-04	
ω_{19}	1.0720e+04	longitudinal mode
α_{19}	5.3599e+00	
ς_{19}	5.0000e-04	
ω_{20}	1.1340e+04	2nd Bending mode
α_{20}	5.6698e+00	
ς_{20}	5.0000e-04	
ω_{21}	1.6690e+04	3rd Bending mode
α_{21}	8.3448e+00	
ς_{21}	5.0000e-04	

TABLE V. The eigenfrequencies and MDRs for the macrobeam with 17 microbeams and air-filled cavity.

Eigen Solution	Acoustic Structure Interaction			Mode shape
	$\eta_{air} = 0.0$	$\eta_{air} = 0.01$	$\eta_{air} = 0.1$	
ω_1	5.8450+03	5.8450e+03	5.8450e+03	
α_1	2.9212+00	2.9466e+00	3.1752e+00	1st Bending mode
ς_1	4.9978e-04	5.0413e-04	5.4323e-04	
ω_2	1.0715e+04	1.0715e+04	1.0715e+04	
α_2	5.3536e+00	5.4292e+00	6.0259e+00	longitudinal mode
ς_2	4.9965e-04	5.0671e-04	5.6238e-04	
ω_3	1.1118e+04	1.1119e+04	1.1149e+04	
α_3	5.1475e+00	1.3373e+01	7.8281e+01	2nd Bending mode (macro)
ς_3	4.6297e-04	1.2028e-03	7.0212e-03	
$\omega_{4\sim19}$	1.1751e+04	1.1751e+04	1.1739e+04	
	~1.1802e+04	~1.1802e+04	~1.1789e+04	
$\alpha_{4\sim19}$	3.7245e+00	4.6748e+01	4.3453e+02	16 microbeam modes
	~3.7311e+00	~4.7127e+01	~4.3822e+02	(1st bending)
$\varsigma_{4\sim20}$	3.1694e-04	3.9781e-03	3.6992e-02	
	~3.1615e-04	~3.9933e-03	~3.7148e-02	
ω_{21}	1.1954e+04	1.1954e+04	1.1911e+04	
α_{21}	4.2201e+00	3.9369e+01	3.6536e+02	2nd Bending mode (micro)
ς_{21}	3.5302e-04	3.2934e-03	3.0660e-02	
ω_{22}	1.6696e+04	1.6696e+04	1.6695e+04	
α_{22}	8.3301e+00	8.6830e+01	1.1818e+01	3rd Bending mode
ς_{22}	4.9864e-04	5.2008e-04	7.0789e-04	

increased due to air dissipation. The MDRs for the ASI model with $\eta_{air} = 0.01$ and $\eta_{air} = 0.1$ are 1.8891e-03 and 1.3459e-02, respectively. This is about 140% and 1304% improvements, respectively. For the 21nd eigenfrequency the improvements are even larger and close to the values for the pure microbeam modes.

It is also observed that the MDR for the 2nd eigenfrequency of the macrobeam, which is a longitudinal mode, has increased slightly in case of the ASI with dissipation. However, the enhancement is much lower than for the second bending mode of the macrobeam even if its eigenfrequency is close to the first bending mode of the microbeam. However, the longitudinal motion of the macrobeam does not excite the microbeam bending motion. We also see that the MDR for the 3rd bending mode is only slightly increased, since there is no microbeam mode in the vicinity.

We also perform a time-harmonic analysis of the macrobeam with multiple microbeams. As seen in Figure 8, a force is applied with 1 N and the magnitude of y-displacement is examined at the response measuring point positioned at the bottom right corner. The frequency spans a range from 1.05e+04 to 1.25e+04 [rad/s] computed at 2π [rad] intervals, which covers the first 22 eigenfrequencies including the longitudinal mode, the 2nd bending mode of the microbeam, and the 1st bending mode of the microbeam. The results appear in Figure 8. In the void model, we note the resonance peak for the 2nd bending mode corresponding to the eigenfrequencies discussed in Table IV and also the very flat resonance peak for the longitudinal mode due to the measuring of the y-displacement only. The increase in MDRs due to the air dissipation is clearly noted for both modes involving the 2nd macrobeam bending motion.

To study the effect of the positioning of the microbeams, the time-harmonic analysis is repeated with the 17 microbeam resonators randomly distributed. We set the range of random location change within $\Delta x = \Delta y = \pm 2$ mm. Figure 9 shows the corresponding frequency response. When comparing the result of the macrobeam with evenly distributed microbeams, a very similar response is observed. Only the resonance peaks are slightly shifted upward due to the slightly different effective stiffness of the macrobeam.

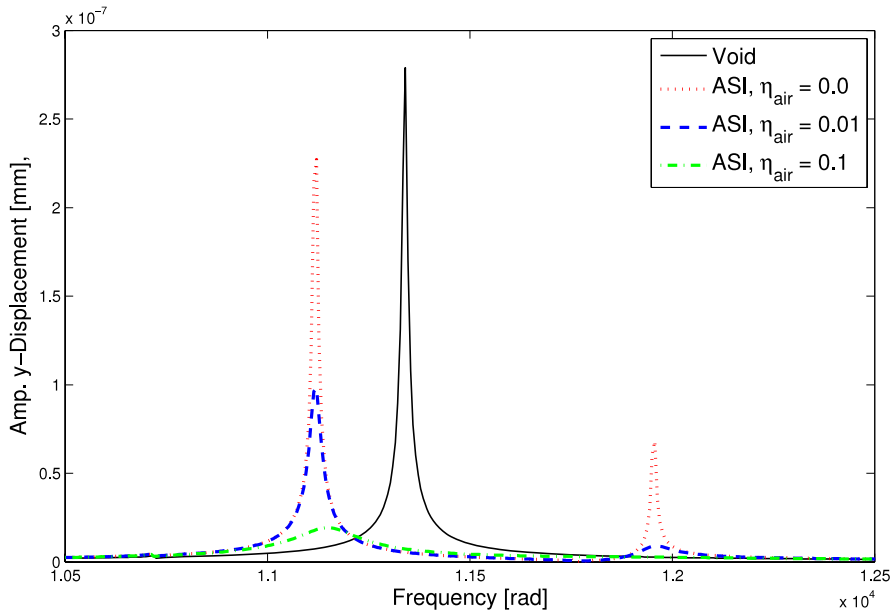

FIG. 8. Frequency responses for the macrobeam with multiple microbeam resonators.

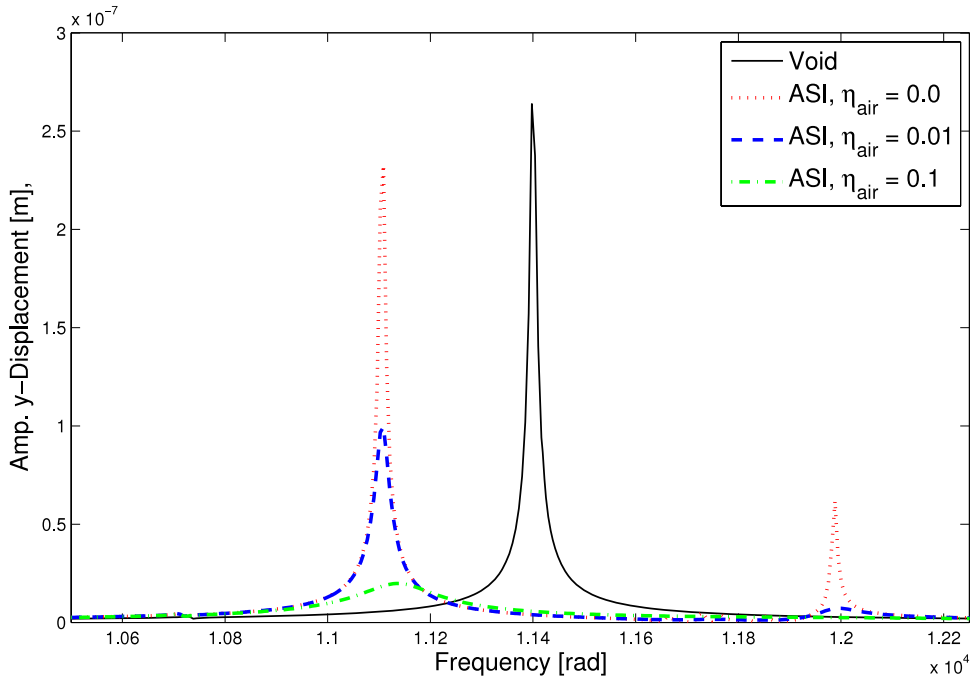

FIG. 9. Frequency responses for the macrobeam with randomly distributed microbeam resonators.

We expect a larger difference if we not only have a random location of the microbeams, but also consider a random thickness of the microbeam resonators. In this case not all microbeams are in resonance with the macrobeam motion and we expect the enhancement of damping to be smaller. Each thickness is changed randomly within the range ±0.01 mm. The results appear in Figure 10. In comparison with the results seen in Figure 8, because of both randomness in the locations and thicknesses of the microbeams, the frequencies for the resonance are changed and we see also that the resonance peaks are less damped as expected.

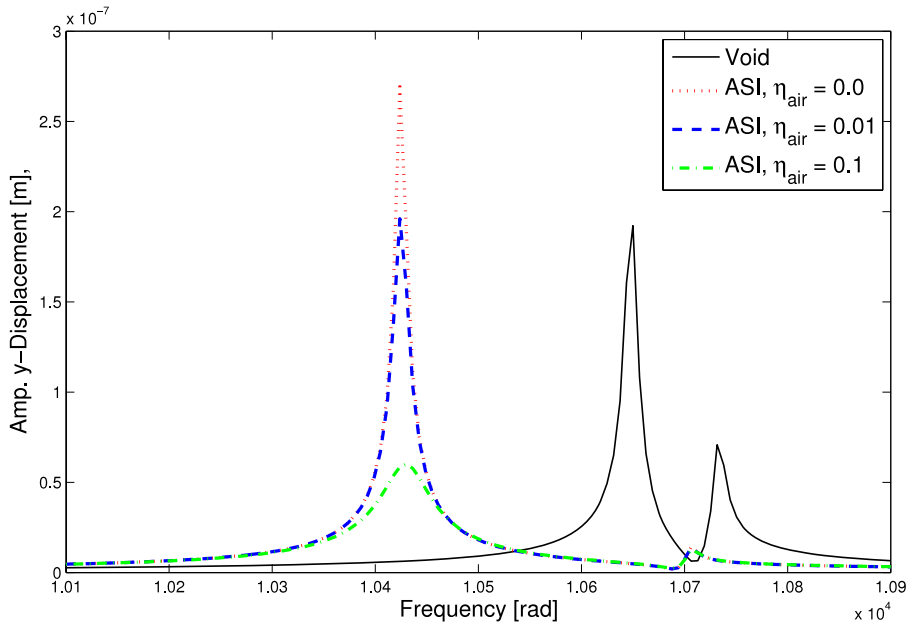

FIG. 10. Frequency responses for the macrobeam with randomly distributed microbeam resonators with random thickness.

D. Numerical experiment with the thermoacoustic-structure interaction model

Until now, we have studied the lossy acoustic media using the complex speed of sound. In order to compare this phenomenological model with a more realistic lossy acoustic model, we again examine the numerical example discussed in Section III.B by employing the thermoacoustic-structure interaction model.

The losses occur in the acoustic thermal and viscous boundary layers near the walls and become especially important in geometries with small dimensions. For the considered materials the

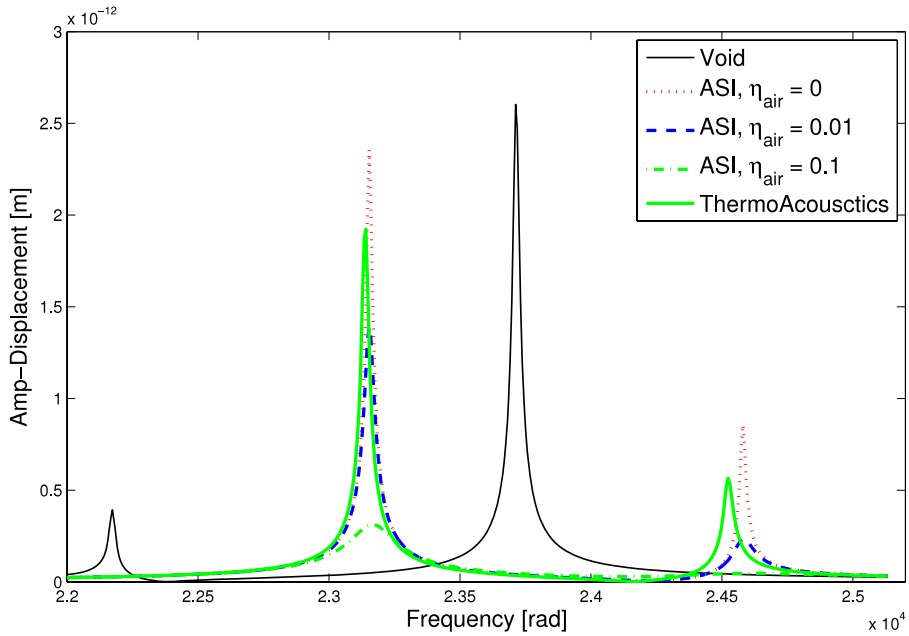

FIG. 11. Comparison the frequency responses seen in Figure 7 with the frequency response obtained by using thermoacoustics.

dimensions of microbeams and acoustic cavities is sufficiently small so that a thermoacoustic model becomes relevant. Different from normal acoustics analysis considering isentropic and lossless governing equations, the thermoacoustic formulation takes the dissipative effects of viscous shear and conduction into account. We use the thermoacoustic-structure interaction model in COMSOL Multiphysics using standard properties for air (with zero bulk viscosity). We employ a very fine mesh near isothermal boundaries, i.e. boundaries between the structure and the acoustic domain, to be able to accurately solve for the viscous and thermal boundary layers and the resulting acoustic damping. For a detailed discussion of the analysis of the thermoacoustics we refer to the user's guide of COMSOL.[17]

As in Section III.B, we perform a time-harmonic analysis of the macrobeam with a single microbeam and study the frequency responses with the thermoacoustic-structure interaction model. The geometry and all other parameters are unchanged compared to the previous analysis. From the results shown in Figure 11 we can see that the frequency response curve obtained with the thermoacoustic model, is qualitatively similar to the one obtained with the phenomenological damping model. With respect to the dissipation level it appears that the effect is somewhat smaller than the one corresponding to $\eta_{air} = 0.01$. Additionally, we see a small frequency shift.

It should be emphasized that the computational cost associated with the full thermoacoustic analysis is significantly higher than the one needed when using the simple complex sound speed. Thus, the results indicate that the simple model can be advantageously be used for a first estimation of the effect of the ASI with acoustic dissipation.

IV. CONCLUSION

In this paper we have studied the possible enhancement of macroscopic damping ratios by embedded microbeams vibrating in a lossy acoustic medium. The study encompassed the derivation of a simple theoretical model and a computational FE study using an acoustic-structure interaction model. The dissipation in the internal acoustic cavities was accounted for using a phenomenological model with a complex speed of sound and was also compared to a more advanced thermoacoustic-structure interaction analysis.

The theoretical model established the connection, under a number of simplifications, between an increased damping ratio of the microbeams and the resulting enhanced damping ratio of the macrobeam. The results indicated that an increased damping due to acoustic-structure interaction in internal air cavities could cause an increased overall damping ratio, as was observed experimentally for beams of porous materials. The computational FE study supported this conclusion both for the case of a single and multiple microbeams. In both cases, significant enhancement of the damping ratio was observed when we applied losses in the acoustic model for the internal air cavities. In the case where we applied randomness in the location and the thickness of the microbeams, we found that the location of the microbeams did not affect the damping properties, whereas reduced damping was observed when all microbeams were not alike and tuned with the macrobeam frequency. Finally, we demonstrated qualitative similarities between the time-harmonic response behavior when employing the simple, and computationally cheap phenomenological loss model, and the full thermoacoustic-structure interaction model.

As a next step, current work is in progress on optimizing the geometry of the microbeams in order to maximize the internal damping ratio. As we predict from this study, this will then reflect in an increased modal damping ratio of finite devices made of porous material and thus extending the possibilities for industrial applications.

ACKNOWLEDGMENTS

We would like to thank out colleague Casper Schousboe Andreasen for providing us with the experimental data and figures. The work was funded by the Danish Research Agency through the innovation consortium FMAT.

[1] C. S. Andreasen, "Damping in porous beams," *Technical Report* (Technical University of Denmark, 2011).

[2] J. P. Den Hartog, *Mechanical Vibrations* (McGraw-Hill, New York, 1934).
[3] T. Asami and O. Nishihara, J. Vib. Acoust **125**, 398 (2003).
[4] R. Viguie and G. Kerschen, "The Nonlinear Tuned Vibration Absorber," in *MATEC Web of Conferences*, edited by M. Belhaq and R. Ibrahim (2012), Vol. 1, p. 05007.
[5] M. Strasberg and D. Feit, J. Acoust. Soc. Am **99**(1), 335 (1996).
[6] R. J. Nagem, I. Veljkovic, and G. Sandri, J. Sound Vib **207**(3), 429 (1997).
[7] Z. Liu, X. Zhang, Y. Mao, Y. Y. Zhu, Z. Yang, C. T. Chan, and P. Sheng, Science **289**, 1734 (2000).
[8] J. Mei, G. Ma, M. Yang, Z. Yang, W. Wen, and P. Sheng, Nature Communications **3**, 756 (2012).
[9] L. Brillouin, *Wave Propagation in Periodic Structures* (Dover Publications Inc, New York, 1953).
[10] D. L. Yu, Y. Z. Liu, G. Wang, L. Cai, and J. Qiu, Phys. Lett. A **348**, 410 (2005).
[11] H. H. Huang, C. T. Sun, and G. L. Huang, Int. J. Eng. Sci **47**, 610 (2009).
[12] J. S. Jensen, J. Sound Vib **266**, 1053 (2003).
[13] B. S. Lazarov and J. S. Jensen, Int. J. Non-linear Mech **42**, 1186 (2007).
[14] M. I. Hussein and M. J. Frazier, J. Sound Vib **332**(20), 4767 (2013).
[15] M. I. Hussein, M. J. Leamy, and M. Ruzzene, Appl. Mech. Rev **66**(4), 040802 (2014).
[16] H. Hosaka, K. Itao, and S. Kuroda, Sensor Actuat A-Phys **49**, 87 (1995).
[17] COMSOL Reference Manual for COMSOL 4.4.